American Mineralogist, Volume 89, pages 339–347, 2004

Spriggite, $Pb_3[(UO_2)_6O_8(OH)_2](H_2O)_3$, a new mineral with β-$U_3O_8$–type sheets: Description and crystal structure

JOËL BRUGGER,[1,2,*] SERGEY V. KRIVOVICHEV,[3,†] PETER BERLEPSCH,[4] NICOLAS MEISSER,[5,6] STEFAN ANSERMET,[5] AND THOMAS ARMBRUSTER[4]

[1]School of Earth and Environmental Sciences, The University of Adelaide, North Terrace, 5005 Adelaide, South Australia
[2]Division of Mineralogy, South Australian Museum, North Terrace, 5000 Adelaide, South Australia
[3]Mineralogisch-Petrographisches Institut, Kiel Universitaet, Olshausenstrasse 40, 24118 Kiel, Germany
[4]Laboratorium für Chemische und Mineralogische Kristallographie, Universität Bern, Freiestrasse 3, CH-3012 Bern, Switzerland
[5]Musée Géologique Cantonal UNIL-BFSH2, CH-1015 Lausanne-Dorigny, Switzerland
[6]Laboratoire des Rayons-X, Institut de Minéralogie et de Géochimie, UNIL-BFSH2, CH-1015 Lausanne-Dorigny, Switzerland

ABSTRACT

Spriggite, $Pb_3[(UO_2)_6O_8(OH)_2](H_2O)_3$, is a new hydrated Pb uranyl oxyhydroxide found near Arkaroola, Northern Flinders Ranges, South Australia. The new mineral's name honors geologist and conservationist Reginald Claude Sprigg (1919–1994), founder of the Arkaroola Tourist Station. Together with beta-uranophane, soddyite, kasolite, Ce-rich francoisite-(Nd), metatorbernite, billietite, Ba-bearing boltwoodite, schoepite, metaschoepite, and weeksite, spriggite results from the supergene alteration of U-Nb-REE-bearing hydrothermal hematite breccia. Spriggite forms prismatic crystals up to about 150 μm in length and up to 40 μm across. It is transparent, bright orange in color with vitreous luster, biaxial, n_{min}= 1.807; n_{max} = 1.891 (Na_D, 22.5 °C), non-fluorescent, brittle with an uneven fracture. It has a pale orange streak, Mohs' hardness ~4, good cleavage along (100) and D_{calc} = 7.64(6) g/cm^3. The empirical formula is $(Pb_{2.77}Ca_{0.06}Ba_{0.04})_{\Sigma 2.87}U_6O_{19.9}(OH)_2 \cdot 3H_2O$, and the simplified formula is $Pb_3[(UO_2)_6O_8(OH)_2](H_2O)_3$. Spriggite is monoclinic, $C2/c$, a = 28.355(9), b = 11.990(4), c = 13.998(4) Å, β = 104.248(5); V = 4613(3) Å^3, Z = 8. The strongest eight lines in the powder X-ray diffraction pattern are [d in Å (I)(hkl)]: 6.92(60)(400), 6.02(30)(11$\bar{2}$;020), 3.46(80)(800), 3.10(100)(204;$\bar{6}$04;3$\bar{3}$2;$\bar{5}$32), $\bar{2}$.74(30)($\bar{4}$40), 2.01(30)(33$\bar{6}$), 1.918(60)(10.0$\bar{4}$;14.0$\bar{4}$;11.$\bar{3}$2;$\bar{1}\bar{3}$.31), 1.738(30)(5$\bar{3}$6;$\bar{1}\bar{1}$.36). The structure has been solved from a crystal twinned on (001) and refined to R1 = 9.7%. The structure is based upon the $[(UO_2)_6O_8(OH)_2]^{6+}$ sheets of uranyl polyhedra of the β-U_3O_8 anion topology with Pb^{2+} cations and H_2O groups in the interlayer. Billietite and spriggite contain only hexavalent U in the uranyl sheets, whereas the similar sheets in β-U_3O_8 contain U^{5+} and U^{6+}, and those in ianthinite U^{4+} and U^{6+}. Spriggite has the highest Pb:U ratio among the known hydrated Pb uranyl oxyhydroxide minerals.

INTRODUCTION

The alteration of primary U^{4+}-containing ores results in complex mineral assemblages characterized by many uranyl-bearing phases (see Finch and Murakami 1999, for a recent review). Over the past decades, several mineralogical studies have been devoted to the alteration of U-deposits as natural analogs to radioactive waste repositories. Ultimately, these studies will allow the calibration of geochemical numerical models for the prediction of mass transport around natural and artificial U-bearing materials over geological time scales (Colon et al. 2001; Ewing 1993; Miller et al. 2000). A better understanding of element mobility around ore deposits also has consequences for geochemical prospecting for ore deposits under regolith cover (e.g., Smith 1996).

This communication is part of an on-going investigation of the timing and geochemistry of U and rare-earth element (REE) mobility in and around the Mt. Painter inlier, South Australia. We present mineralogical data on a new hydrated Pb uranyl oxyhydroxide discovered in the alteration zone of a hydrothermal hematite-U-Nb-REE deposit from the Mt Painter inlier. The new mineral was named spriggite to acknowledge the contribution of Reginald Claude Sprigg (1919–1994) to the understanding and development of the geological, ecological, and historical resources of the Arkaroola station, the type locality of spriggite. In 1944, Dr. Sprigg joined the South Australian Geological Survey to reactivate the Radium Hill U mining field and regionally map the Mt. Painter U field. In 1967, he purchased, with his family (who still lives there) the 61 000 hectares Arkaroola sheep station and operated it in the interests of wildlife conservation and preservation of its unique flora, and its mining and pastoral history.

In recent years, the chemical and structural features of uranyl oxide hydrates have received considerable attention, due to their importance for the understanding of the alteration of spent nuclear fuel under oxidizing conditions (Finch and Ewing 1992). In recent ground-breaking studies, Burns and co-authors provided important new information about the crystal structures

* E-mail: joel.brugger@adelaide.edu.au
† Permanent address: Department of Crystallography, Faculty of Geology, St. Petersburg State University, University Emb. 7/9, 199034 St. Petersburg, Russia

of the Pb uranyl oxide hydrates vandenriesscheite (Burns 1997), richetite (Burns 1998), masuyite (Burns and Hanchar 1999), and wölsendorfite (Burns 1999b; see Table 1 for chemical formulae). The crystal-chemical variability in curite and fourmarierite have been characterized in detail by Li and Burns (2000a, 2000b; Table 1). In the present work, we will show that the structure of spriggite is closely related to the structures of known hydrated Pb uranyl oxyhydroxides and provides additional information for understanding stability and evolution of hydrated Pb uranyl oxyhydroxides during oxidation of U^{4+} phases.

Occurrence

Spriggite occurs at the Number 2 workings on Radium Ridge near Mt. Painter, near Arkaroola, Northern Flinders Ranges, South Australia. The Proterozoic basement of the Mt. Painter inlier contains granites and gneisses highly enriched in U and Th (10–100 ppm). The radiogenic heat produced by these granites has been responsible for a long-lasting thermal anomaly, which has driven—and still drives—hydrothermal activity in and around the inlier (Sandiford et al. 1998). Although accurately dating the various hydrothermal deposits located in and around the inlier remains a major challenge, available data suggest a long and complex history consistent with the unusual thermal history of the inlier. The following age estimates are available: (1) small hematite-U ± Cu-Nb-REE deposits, such as the one exploited at the Number 2 workings, locally contain abundant primary monazite-(Ce) that gives an approximate Pb-Pb age of 460 Ma (Elburg et al. in press); (2) part of a large epithermal system characterized by quartz ± hematite, fluorite, carbonate, barite, laumontite veins and breccias seems to have formed around 450 ± 50 Ma (Elburg et al. 2003); (3) sinter deposits around Mt. Painter have a primary Permo-Carboniferous paleomagnetic age (Idnurm and Heinrich 1993); (4) economic concentrations of U in the Tertiary sediments surrounding the Mt. Painter inlier, i.e., the Beverley U mine, resulted from the remobilization of U from the inlier during or after fluvial Tertiary sedimentation (Walker 1999); and (5) the active Paralana hot spring represents the last visible remnant of hydrothermal activity around the Mt. Painter Inlier. The spring is located at the intersection of a major regional fault (Paralana fault) and one or two smaller faults. Apatite fission-track thermochronology suggests pervasive hydrothermal activity during mid-Tertiary along the Paralana Fault zone (Foster et al. 1994).

At the Number 2 workings, a massive U-Nb-REE-bearing hematite-quartz breccia is crosscut by epithermal quartz mineralization. Small-scale exploitation of Ra took place here at the turn of the century (Coats and Blissett 1971). The hematite-quartz breccia at Number 2 contains a magmatic-hydrothermal mineral assemblage including monazite-(Ce), xenotime-(Y), a metamict and highly altered Fe-U-Nb-rich euxenite-group mineral, fluorapatite, and a hydrated Fe-phosphate with empirical formula $FePO_4 \cdot 2\text{-}2.5H_2O$, growing expitaxially with fluorapatite (phosphosiderite?). The primary hydrothermal assemblage also contains an unidentified mineral forming prismatic striated crystals with rounded triangular sections morphologically similar to tourmaline. The crystals of this unknown primary U-mineral reach in excess of one centimeter in length and diameter, and usually are altered to a mixture of soddyite $[(UO_2)_2SiO_4 \cdot 2H_2O$, >50 vol%], beta-uranophane $[Ca(UO_2)_2(SiO_3OH)_2 \cdot 5H_2O]$, billietite $[Ba(UO_2)_6O_4(OH)_6 \cdot 4H_2O]$, schoepite $[(UO_2)_8O_2(OH)_{12} \cdot 12H_2O]$ and metaschoepite $[(UO_2)_8O_2(OH)_{12} \cdot 10H_2O]$, rutherfordine $[(UO_2)CO_3]$, and locally spriggite. Other secondary minerals occurring in the vugs of the epithermal quartz or replacing primary U-minerals in the hematite breccia include kasolite $[Pb(UO_2)SiO_4 \cdot H_2O]$, Ce-rich francoisite-(Nd) $[(Nd,Ce)(UO_2)_3(PO_4)_2O(OH) \cdot 6H_2O]$, metatorbernite $[Cu(UO_2)_2(PO_4)_2 \cdot 8H_2O]$, Ba-bearing boltwoodite $[(K,Ba)(UO_2)(SiO_3OH)(H_2O)_{1.5}]$, weeksite $[K_2(UO_2)_2(Si_5O_{13}) \cdot 13H_2O]$, an acicular curite-like mineral (from powder XRD), and barite. Spriggite replaces the unknown primary mineral in highly radioactive blocks of ore. The least altered crystals of the primary U-mineral retain a black color, with a matte luster and a granular fracture. However, polished sections reveal that the mineral consists of a mixture of a Mn-Pb oxyhydroxide, uranyl oxyhydroxides, and hydrated uranyl-lead oxyhydroxides. The Mn-Pb oxide is probably cesarolite; it contains an average of 51.8 wt% MnO_2 and 27.9 wt% PbO, and small quantities of Ce_2O_3 (0.43 wt%), Nd_2O_3 (0.18 wt%), FeO (0.62 wt%), Al_2O_3 (0.26 wt%) and SiO_2 (0.34 wt%) (average over 9 analyses). Highly variable U contents up to 8.80 wt% UO_3 are probably related to inclusions.

Spriggite is the only red-orange mineral found at Mt. Painter, and hence is likely to correspond to the "uranosphaerite" reported by Coats and Blissett (1971) from the Number 2 workings. No Bi has been detected in the minerals from the Number 2 workings, and Coats and Blissett (1971) probably based their determination simply on color. A search of the Mines Department collection, now hosted at the South Australian Museum, failed to reveal a sample of "uranosphaerite."

The new mineral and its name have been approved by the International Mineralogical Association (proposal 2002-014). The type material is deposited at the Musée géologique cantonal, Lausanne, Switzerland (Holotype specimen MGL68937). The co-type is de-

TABLE 1. Compositional data for hydrated Pb uranyl oxyhydroxides minerals

Mineral	Formula*	Pb:U	U:(charge)	$^{VI}U:^{VII}U$	O:OH	Ref.
vandenriesscheite	$Pb_{1.57}[(UO_2)_{10}O_6(OH)_{11}](H_2O)_{11}$	1:6.36	1:0.30	no ^{VI}U	1:1.83	1
fourmarierite	$Pb[(UO_2)_4O_3(OH)_4](H_2O)_4$	1:4.00	1:0.50	no ^{VI}U	1:1.33	2, 3
richetite	$M_xPb_{8.57}[(UO_2)_{18}O_{18}(OH)_{12}]_2(H_2O)_{41}$	1:4.15	1:0.47	no ^{VI}U	1:0.67	4
masuyite	$Pb[(UO_2)_3O_3(OH)_2](H_2O)_3$	1:3.00	1:0.67	no ^{VI}U	1:0.67	5
curite	$Pb_3[(UO_2)_8O_8(OH)_6](H_2O)_3$	1:2.67	1:0.75	1:3.00	1:0.75	6,7
sayrite	$Pb_2[(UO_2)_5O_6(OH)_2](H_2O)_4$	1:2.50	1:0.80	1:4.00	1:0.33	8
wölsendorfite	$Pb_{6.16}Ba_{0.36}[(UO_2)_{14}O_{19}(OH)_4](H_2O)_{12}$	1:2.15	1:1.00	1:3.67	1:0.21	9
spriggite	$Pb_3[(UO_2)_6O_8(OH)_2](H_2O)_3$	1:2.00	1:1.00	1:2.00	1:0.25	10

Notes: 1 = Burns 1997; 2 = Piret 1984; 3 = Li and Burns 2000b; 4 = Burns 1998; 5 = Burns and Hanchar 1999; 6 = Mereiter 1979; 7 = Li and Burns 2000a; 8 = Piret et al. 1983; 9 = Burns 1999b; 10 = this work.
* Formula of the sheet is given in square brackets.

posited at the South Australian Museum, Adelaide, South Australia (specimen G27305).

Appearance, physical, and optical properties

Spriggite forms aggregates of randomly oriented prismatic crystals that can reach more than a centimeter in size. The individual crystals measure up to about 150 μm in length, with sections up to 40 × 40 μm^2. The morphology of the crystals is dominated by the {100} prism; they also display another prominent pinacoid and four small terminal faces (Fig. 1). Spriggite commonly displays twinning by penetration: three individuals are separated by a ~60° rotation around [100] to form a six-legged star similar to the "sagenite" twin of rutile (Fig. 1). Spriggite also occurs as spherical nodules measuring between 0.5 and 3 mm in diameter and included in massive soddyite. The nodules have a conchoidal fracture and an adamantine luster reminiscent of crocoite. Spriggite is easily recognized by its bright orange color. The streak is pale orange. Spriggite is transparent with a vitreous luster, and displays no fluorescence under UV light. Optically, spriggite is biaxial, with n_{min}= 1.807 and n_{max} = 1.891 (Na_D, 22.5 °C). It displays a strong pleochroism from pale yellow to dark orange. The mineral has a Mohs' hardness of about 4 and a good cleavage along (100) (Fig. 1). It is brittle with an uneven fracture. Spriggite sinks in Clerici solution (density = 4.4 g/cm^3), in accord with the calculated density of 7.64(6) g/cm^3. The density has been calculated assuming a water content of 4 H_2O per formula unit (pfu), and a cell volume of 4612.68 Å^3; the uncertainty reflects the range of compositions provided by the electron microprobe analyses (Table 1).

Chemical composition and IR spectrum

Electron microprobe analyses (Table 2) were performed on the CAMECA SX-50 electron microprobe of Adelaide Microscopy (Adelaide University), operated in WDS mode at 15 kV and 20 nA, with a tightly focused beam scanned over a surface of about 20 μm^2. The following X-ray lines and standards were used: U*M*α-uranium metal; Pb*M*α-crocoite; Ca*K*α-wollastonite; Ba*L*α-barite. Additional measured elements include: K_2O (≤0.25 wt%), TiO_2 (≤0.11 wt%), FeO, SrO, Na_2O, and SiO_2 (all < 0.05 wt%). These analyses show that spriggite is a relatively pure hydrated Pb uranyl oxyhydroxide, with the following empirical formula calculated assuming 6 U and 8 H pfu: $(Pb_{2.77}Ca_{0.06}Ba_{0.04})_{\Sigma 2.87}U_6O_{19.9}(OH)_2 \cdot 3H_2O$.

The FT-IR spectrum of spriggite, collected using a diamond cell GRAESEBY SPECAC/PARAGON 1000 (University of Lausanne) on ground material for wavenumbers between 600 and 4000 cm^{-1}, shows a broad asymmetric stretching mode of H_2O (υH_2O) centered around 3200 cm^{-1} (Fig. 2). The width of the υH_2O band (3620 cm^{-1} to ~2700 cm^{-1}) indicates a complex network of hydrogen bonding in this mineral. A band at 1620 cm^{-1} with a shoulder at 1584 cm^{-1} corresponds to the bending vibrations (δH_2O). The absorption between 750 and 800 cm^{-1} probably correspond to asymmetric stretching (υ_3) and/or symmetric stretching (υ_1) of the uranyl ion (UO_2^{2+}; Cejka 1999).

Powder x-ray diffraction

The powder X-ray diffraction (XRD) pattern of spriggite (Table 3) was obtained using a 114.6 mm diameter Gandolfi camera operated at 40kV and 30mA (Ni-filtered Cu*K*α radiation, 99 h exposure time). The strongest eight lines in the powder XRD pattern are [*d* in Å (*I*)(*hkl*)]: 6.92(60)(400), 6.02(30)(11$\bar{2}$;020), 3.46(80)(800), 3.10(100)(204;$\bar{6}$04;3$\bar{3}$2;$\bar{5}$32), 2.74(30)($\bar{4}$40), 2.01(30)(33$\bar{6}$), 1.918(60)(10.0$\bar{4}$;14.0$\bar{4}$;11.$\bar{3}$2;$\bar{1}$3.31), and 1.738(30)(5$\bar{3}$6;$\bar{1}$1.36).

Crystal structure

Data collection

Selection of a crystal appropriate for data collection was a challenge due to the twinning of the spriggite crystals. A crystal with approximate dimensions 0.12 × 0.12 × 0.04 mm^3 was mounted on a Bruker Platform 3-circle goniometer equipped with a 1K SMART CCD (charge-coupled device) detector. The data were collected using monochromatic Mo*K*α X-radiation and frame widths of 0.3 in ω. Unit-cell dimensions (Table 4) were refined on the basis of 689 reflections using least-squares techniques. More than a hemisphere of three-dimensional data was collected for 2.27 ≤ θ ≤ 27.79; the intensities were integrated and corrected for Lorentz, polarization, and background effects using the Bruker program SAINT. An empirical absorption-correction was done on the basis of the intensities of equivalent reflections and reduced R_{INT} of 415 intense reflections from 15.6 to 8.6%. A total of 12 714 reflections were collected and merging of equivalent reflections gave 4910 unique reflections with 2759 classified as observed ($|F_o| \geq 4\sigma_F$).

Structure solution and refinement

Scattering curves for neutral atoms, together with anomalous dispersion corrections, were taken from Ibers and Hamilton (1974). The Bruker SHELXTL Version 5 system of programs was used for the refinement of the crystal structure. Reflection statistics indicated space group *C*2/*c*, which was verified by the successful solution of the structure by direct methods. The structure was refined on the basis of F^2 for all unique data. On the final stage of the refinement, a pseudomerohedral twinning

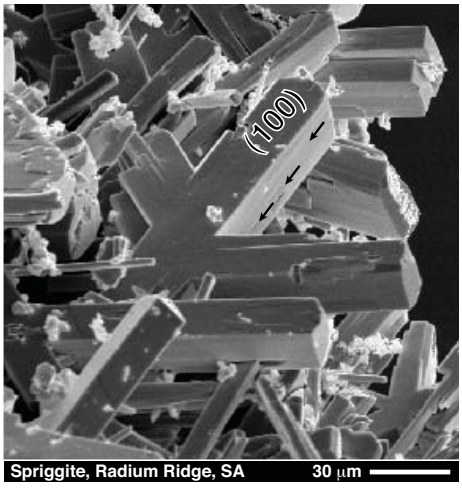

Figure 1. Secondary electron microscope image of spriggite crystals and twins from the Number 2 workings, Radium Ridge, Northern Flinders Ranges, South Australia. The longest crystal is about 90 μm in length. Arrows indicate the trace of the cleavage.

Table 2. Chemical composition of spriggite

	Average	Range
UO_3	70.90	70.00–72.12
PbO	25.51	24.02–26.63
CaO	0.14	<0.05–0.48
BaO	0.25	<0.05–0.85
H_2O_{calc}	2.98	2.94–3.03
Sum	99.78	98.95*–101.04*

Notes: Average of 6 spot analyses. Values in wt%.
* Maximum and minimum analytical totals.

TABLE 3. Powder XRD data for spriggite

d_{obs}	I_{vis}	d_{calc}	I_{calc}	h	k	l	d_{obs}	I_{vis}	d_{calc}	I_{calc}	h	k	l
6.92	60	6.87	100	4	0	0			1.718	17	16	0	0
6.02	30	6.04	18	1	1	$\bar{2}$	1.695	10	1.696	8	0	0	8
		5.99	16	0	2	0			1.695	8	8	0	$\bar{8}$
5.31	5	5.28	10	$\bar{2}$	2	1	1.677	10	1.683	8	2	$\bar{6}$	4
		4.93	10	2	$\bar{2}$	1			1.682	9	6	6	$\bar{4}$
		3.50	35	$\bar{2}$	0	4	1.656	10	1.664	13	1	7	$\bar{2}$
		3.47	61	1	3	$\bar{2}$	1.616	5	1.617	4	3	$\bar{7}$	2
3.46	80	3.44	99	8	0	0			1.617	4	$\bar{5}$	7	2
3.10	100	3.12	54	2	0	4	1.556	5	1.560	3	4	0	8
		3.12	56	$\bar{6}$	0	4			1.559	4	$\bar{12}$	0	8
		3.10	81	3	$\bar{3}$	2	1.542	10	1.542	4	14	0	4
		3.10	79	$\bar{5}$	3	2			1.542	4	7	$\bar{5}$	5
3.01	5	2.99	3	7	$\bar{1}$	2			1.540	6	15	$\bar{3}$	2
		2.99	2	$\bar{9}$	1	2			1.539	7	$\bar{17}$	3	2
		2.98	4	$\bar{8}$	2	0	1.510	5	1.513	4	9	$\bar{3}$	6
2.74	30	2.75	31	$\bar{4}$	4	0			1.512	4	$\bar{15}$	3	6
2.45	20	2.45	7	6	0	4			1.511	4	4	4	$\bar{8}$
		2.45	6	$\bar{10}$	4	4	1.494	10	1.497	7	7	$\bar{7}$	2
		2.44	11	7	$\bar{3}$	2			1.497	6	$\bar{9}$	7	2
		2.44	12	9	3	$\bar{2}$	1.379	5	1.384	2	$\bar{8}$	0	10
2.27	20	2.28	22	2	4	$\bar{4}$			1.383	5	3	1	$\bar{10}$
2.16	5	2.17	3	1	$\bar{1}$	6			1.383	7	$\bar{12}$	4	8
		2.17	3	7	1	$\bar{6}$			1.371	4	14	$\bar{4}$	4
		2.16	2	2	$\bar{4}$	4			1.371	4	0	$\bar{8}$	4
		2.16	2	6	4	$\bar{4}$	1.350	20	1.354	9	1	$\bar{7}$	6
		2.15	2	3	$\bar{5}$	2			1.354	9	$\bar{7}$	7	6
		2.15	2	$\bar{5}$	5	2	1.314	5	1.321	3	5	3	$\bar{10}$
2.01	30	2.01	45	3	3	$\bar{6}$			1.317	4	18	2	3
1.991	10	1.998	14	0	6	0			1.308	12	13	3	6
1.918	60	1.917	14	10	0	$\bar{4}$			1.307	12	$\bar{19}$	3	6
		1.916	15	14	0	$\bar{4}$	1.297	5	1.298	9	5	7	$\bar{7}$
		1.912	23	11	$\bar{3}$	2			1.297	9	9	3	$\bar{10}$
		1.911	21	$\bar{13}$	3	1	1.281	5	1.279	4	18	0	4
1.897	5	1.898	8	6	$\bar{4}$	4			1.279	6	6	$\bar{8}$	4
		1.897	9	10	4	$\bar{4}$	1.193	5	1.195	7	15	$\bar{7}$	2
1.821	5	1.820	9	$\bar{12}$	4	0			1.195	6	$\bar{17}$	7	2
1.738	30	1.738	21	5	$\bar{3}$	6	1.180	5	1.183	8	9	$\bar{7}$	6
		1.738	21	$\bar{11}$	3	6			1.182	8	20	$\bar{4}$	2
1.725	10	1.727	13	8	$\bar{6}$	0			1.181	11	21	1	$\bar{8}$

Notes: Gandolfi camera, 114.6 mm diameter, Cu$K\alpha$/Ni-filtered, 40kV 30mA, 99h exposure time. Calculated values are for the model from the crystal structure refinement (i.e., with the unit-cell refinement from the single crystal data).

was introduced using the matrix [$\bar{1}0\bar{1}$/010/001], which lowered the $R1$ index from approximately 12 to 10%. This twinning is essential, though the refined ratio of twin components was approximately 1:20. (Table 5). The structure solution revealed several interlayer positions that were assigned to either H_2O groups or Pb^{2+} cations on the basis of occupancy refinement, local coordination geometry and electroneutrality requirements. In the final refinement, site occupancy factors for the Pb and some H_2O groups were fixed to achieve electroneutrality of the structure, isotropic displacement parameters were constrained to be of the same value for two groups of the O atoms (O_{Ur} and O_{eq}), and displacement parameters of the H_2O groups and Pb7 atom were fixed to 0.100 Å^2. The final model included all atomic positional parameters, anisotropic displacement parameters for the cations (except low occupied Pb7), isotropic displacement parameters for the O atoms and OH groups, and a weighting scheme of the structure factors. The final agreement index ($R1$) of 9.7% was calculated using the 2759 observed reflections. The atomic-positional parameters and anisotropic-displacement parameters for cations are given in Tables 5 and 6, respectively, and selected bond lengths are given in Table 7. Calculated and observed structure factors are provided in Table 8[1].

TABLE 4. Crystallographic data and refinement parameters for spriggite

a (Å)	28.355(9)	Crystal size (mm^3)	0.12 × 0.12 × 0.04
b (Å)	11.990(4)	D_{calc} (g/cm^3)	7.64
c (Å)	13.998(4)	Total ref.	12714
β (°)	104.248(5)	Unique ref.	4910
V (Å^3)	4613(3)	R_{int} (%)	8.6
Space group	$C2/c$	Unique $\|F_o\| \geq 4\sigma_F$	2759
Z	8	Final $R1$* (%)	9.7
F(000)	8372	$wR2$ (%)	26.9
μ (mm^{-1})	82.006	S†	1.125

* $R1 = \Sigma(|F_o| - |F_c|)/\Sigma|F_o|$.
† $S = [\Sigma w(|F_o| - |F_c|)^2/(m - n)]^{½}$, for m observations and n parameters.

RESULTS

Cation coordination. There are six symmetrically independent U^{6+} cations in the structure, each of which is part of a roughly linear UO_2^{2+} (=*Ur*) uranyl cation. The $U1O_2^{2+}$ and $U2O_2^{2+}$ cations are coordinated in the equatorial plane by four anions each resulting in the UrO_4 tetragonal bipyramids. The U3, U4, U5, and U6 cations are coordinated in the equatorial planes by five anions each, thus forming UrO_5 pentagonal bipyramids.

There are seven symmetrically independent Pb sites in the structure and all of them are occupied only partially. The most highly occupied site is Pb1 (s.o.f. = 0.95) coordinated by nine anions (taking into account half occupancy of the H_2O1 and H_2O4 site) with Pb-ϕ bond lengths (ϕ = O, OH, H_2O) ranging from 2.19 to 3.36 Å. The Pb2, Pb3, Pb5, and Pb7 are coordinated by eight anions each with the Pb-ϕ bond lengths in the range of 2.08–3.01 Å. The Pb4 and Pb6 sites are coordinated by nine and seven anions, respectively, with the Pb-ϕ bond lengths in the range of 2.52–3.23 Å. The coordination of the Pb sites is asymmetric owing to the 6s^2

[1]For a copy of Table 8, Document AM-04-055 contact the Business Office of the Mineralogical Society of America (see inside front cover of recent issue) for price information. Deposit items may also be available on the American Mineralogist web site (see inside back cover of a current issue for a web address).

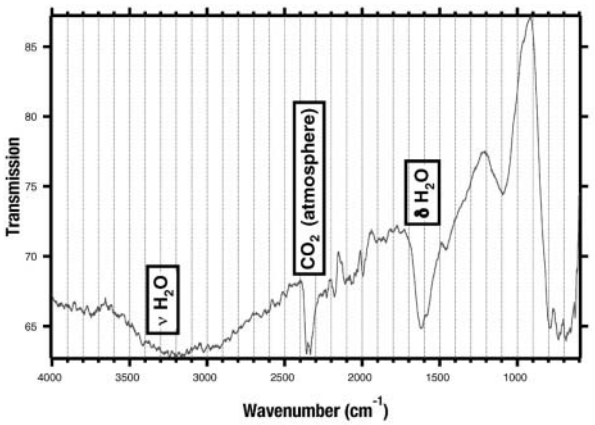

FIGURE 2. IR spectrum of spriggite.

lone-pair electrons on the Pb^{2+} cations.

Bond-valence analysis. Bond-valence sums for the atom sites in the structure of spriggite calculated using bond-valence parameters from Burns et al. (1997a) for the U^{6+}-O bonds, and from Krivovichev and Brown (2001) for the Pb^{2+}-O bonds, are given in Table 5. It should be noted that, due to the low quality of the structure refinement, some cation-anion distances are in error. This problem, and also the essential disorder of the Pb and H_2O positions, make direct bond-valence calculations difficult. Thus, the high bond-valence sums obtained for some O atoms of the uranyl ions (O3, O5, O6, O7, O8, O9, O19, O20, O21, and O22) may be explained by the fact that these atoms form several bonds to the Pb atoms each but, due to the disorder, not all these bonds exist simultaneously at all atom sites. Unfortunately, there is no accepted procedure for bond-valence analysis of disordered configurations. However, in general, the calculated bond-valence sums are in agreement with the expected oxidation states of the cations. The bond-valence sums for the OH16 and OH17 sites are 1.09 and 1.07 valence units (v.u.), which is in agreement with their assignment as hydroxyl groups.

Structure description. The projection of the structure of spriggite on the (010) plane is shown in Figure 3. It is based upon the $[(UO_2)_6O_8(OH)_2]^{6+}$ sheets of uranyl polyhedra shown in Figure 4a. Within the sheets, the UrO_5 pentagonal bipyramids share edges to form chains parallel to the **c** axis. The adjacent chains are linked by sharing edges with UrO_4 square bipyramids. The anion-topology of the $[(UO_2)_6O_8(OH)_2]^{6+}$ sheet, constructed according to the method proposed by Burns et al. (1996), is shown in Figure 4b. It consists of pentagons, squares, and triangles. The pentagons and squares are populated by U atoms, whereas the triangles are empty. This anion topology was named by Burns et al. (1996) as the β-U_3O_8 anion topology. In addition to the structure of β-U_3O_8 (Loopstra 1970), sheets with this anion topology occur in the structure of ianthinite, $[U_2^{4+}(UO_2)_4O_6(OH)_4(H_2O)_4](H_2O)_5$ (Burns et al. 1997b), an early oxidation product of uraninite (Finch and Murakami 1999; Finch and Ewing 1994; Pearcy et al. 1994), and in billietite $Ba[(UO_2)_3O_2(OH)_3]_2(H_2O)_4$ (Pagoaga et al. 1987).

In the structure of spriggite, the $[(UO_2)_6O_8(OH)_2]^{6+}$ sheets are parallel to (100) and are located at the levels of $x \sim 1/8$, 3/8, 5/8, 7/8. The Pb^{2+} cations and H_2O groups are in the interlayer at the

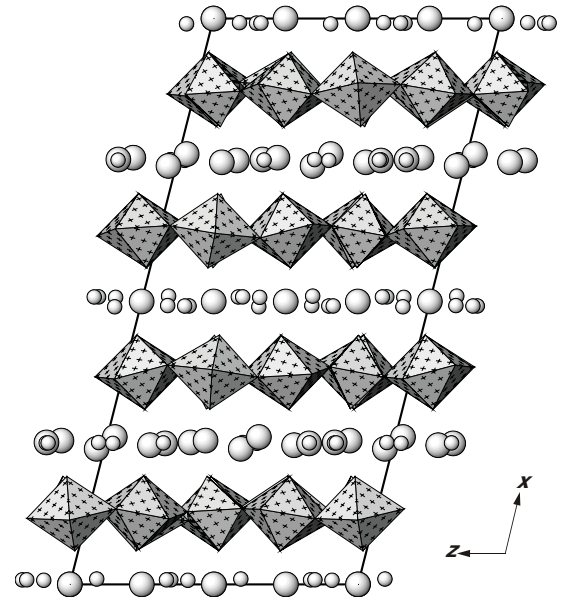

FIGURE 3. Projection of the structure of spriggite on the (010) plane. Uranium polyhedra are cross-hatched; small circles are Pb atoms; large circles are H_2O groups.

levels of $x \sim 0$, ¼, ½, ¾. The interlayers at $x \sim 0$ and ½, and at $x \sim$ ¼ and ¾ are symmetrically distinct (Fig. 5). The interlayers at $x \sim$ ¼ and ¾ contain Pb1, Pb4, and Pb7 sites, and H_2O1, H_2O3 and H_2O4 groups (Fig. 5a). The interlayers at $x \sim 0$ and ½ contain Pb2, Pb3, Pb5, and Pb6 sites, and H_2O2 and H_2O5 groups (Fig. 5b). Though the level of disorder is different for the symmetrically different interlayers, they contain the same number of Pb atoms and H_2O groups, with Pb:H_2O ratio of 1:1.

DISCUSSION

Comparison with β-U_3O_8, billieite and ianthinite

As mentioned above, the sheets of uranyl polyhedra in the structure of spriggite are topologically identical to the sheets of U-O polyhedra in the structures of β-U_3O_8, billietite, and ianthinite. In spriggite, all U atoms are hexavalent, which is evident from the bond-valence and electro-negativity requirements. Billietite also contains hexavalent U in topologically similar layers (Pagoaga et al. 1987). In contrast, in ianthinite, some of the U atoms in square bipyramidal coordinations are U^{4+} (Burns et al. 1997b), whereas in β-U_3O_8, two thirds of the U sites are occupied by U^{5+}, and the remaining one third is occupied by U^{6+} (Loopstra 1970). A related anion topology is found in wyartite $Ca[U^{5+}(UO_2)_2(CO_3)O_4(OH)(H_2O)_7$ (Burns and Finch 1999). However, the square bipyramidal site is replaced by a 7-coordinated site that contains U^{5+}.

The sheets of UO_n polyhedra in the structures of spriggite, billietite, ianthinite, and β-U_3O_8 are metrically similar. The sheet in spriggite has dimensions $c \times b = 13.998 \times 11.990$ Å^2, in billietite $c \times a = 7.1455 \times 12.072$ Å^2, in ianthinite: $a \times b = 7.178 \times 11.473$ Å^2, in β-U_3O_8: $a \times b = 7.069 \times 11.445$ Å^2. Thus in spriggite, the parameter parallel to the elongation of the chains of edge-sharing pentagonal bipyramids (the c parameter) is twice the repeat in

TABLE 5. Atomic position parameters, equivalent isotropic-displacement parameters (Å²) and bond valence sums* (BVS, v.u. (valence units)) for the structure of spriggite

	s.o.f.	*x*	*y*	*z*	U_{eq}	BVS*
U1	1	0.12526(5)	0.50029(12)	0.06516(11)	0.0140(4)	6.28
U2	1	0.12394(5)	–0.00013(14)	–0.18999(11)	0.0145(4)	6.45
U3	1	0.12656(5)	0.30570(14)	–0.18581(10)	0.0156(4)	6.29
U4	1	0.12454(5)	–0.30597(14)	–0.18644(10)	0.0156(4)	5.97
U5	1	0.12421(5)	0.19495(13)	0.06122(11)	0.0141(4)	6.14
U6	1	0.12516(5)	0.80571(13)	0.06188(11)	0.0144(4)	5.95
Pb1	0.95†	0.24991(6)	0.36349(14)	–0.29355(12)	0.0181(4)	2.29
Pb2	0.64†	0.00727(9)	–0.3563(3)	–0.4060(2)	0.0347(8)	1.43
Pb3	0.50†	0.00801(12)	0.1418(4)	–0.3314(3)	0.0316(9)	1.33
Pb4	0.50†	0.25059(13)	0.3412(3)	0.0248(3)	0.0253(8)	1.26
Pb5	0.22†	0.0081(3)	–0.1586(9)	–0.3468(7)	0.040(2)	1.39
Pb6	0.14†	0.0094(5)	–0.3548(17)	–0.5894(14)	0.057(5)	1.42
Pb7	0.05†	0.2500(8)	0.6392(20)	–0.3004(17)	0.010†	2.28
O1	1	0.1318(11)	–0.1379(30)	–0.0963(23)	0.032(2)‡	2.04
O2	1	0.1127(12)	0.3616(31)	0.1436(25)	0.039(3)§	2.03
O3	1	0.0595(11)	0.1953(28)	0.0130(23)	0.032(2)‡	2.46
O4	1	0.1912(11)	0.8139(29)	0.1059(22)	0.032(2)‡	2.01
O5	1	0.0605(11)	0.7941(29)	0.0145(22)	0.032(2)‡	2.27
O6	1	0.0588(12)	–0.3071(30)	–0.2001(24)	0.039(3)§	2.21
O7	1	0.0628(12)	0.3058(31)	–0.2080(24)	0.039(3)§	2.43
O8	1	0.1933(12)	0.4890(30)	0.1207(25)	0.039(3)§	2.34
O9	1	0.1919(12)	0.0017(29)	–0.1800(25)	0.039(3)§	2.29
O10	1	0.1336(11)	0.6486(28)	–0.0311(24)	0.032(2)‡	1.99
O11	1	0.1921(12)	–0.2963(30)	–0.1673(24)	0.039(3)§	1.80
O12	1	0.1327(11)	0.1361(30)	–0.0964(23)	0.032(2)‡	2.06
O13	1	0.1277(11)	0.3642(30)	–0.3452(23)	0.032(2)‡	2.10
O14	1	0.1366(11)	0.3456(28)	–0.0271(24)	0.032(2)‡	1.98
O15	1	0.1152(12)	0.1543(29)	–0.2876(23)	0.032(2)‡	1.99
OH16	1	0.1129(12)	0.5024(27)	–0.2011(23)	0.032(2)‡	1.09
OH17	1	0.1108(12)	0.0004(27)	0.0520(23)	0.032(2)‡	1.07
O18	1	0.1150(12)	0.1628(28)	0.2074(23)	0.032(2)‡	2.04
O19	1	0.0612(12)	–0.0042(29)	–0.2186(24)	0.039(3)§	2.63
O20	1	0.1920(11)	0.2979(28)	–0.1602(23)	0.032(2)‡	2.41
O21	1	0.1913(8)	0.1989(31)	0.1059(23)	0.039(3)§	2.23
O22	1	0.0594(12)	0.5057(30)	0.0109(26)	0.039(3)§	2.43
H_2O1	0.50†	0.2494(49)	0.5136(66)	–0.2043(75)	0.100†	0.77
H_2O2	1	0.0000	0.0000	–0.5000	0.100†	0.33
H_2O3	1	0.2379(21)	0.3581(52)	–0.4772(42)	0.100†	0.34
H_2O4	0.50†	0.2467(48)	0.5053(103)	–0.1564(89)	0.100†	0.36
H_2O5	1	0.0000	-0.4937(69)	–0.7500	0.100†	0.35

* Calculated using bond-valence parameters from Burns et al. (1997a) for the U^{6+}-O bonds and from Krivovichev and Brown (2001) for the Pb^{2+}-O bonds.
† Fixed during final refinement.
‡,§ Constrained to be equal during refinement.

TABLE 6. Anisotropic-displacement parameters (Å²) for the cations in the structure of spriggite

	U_{11}	U_{22}	U_{33}	U_{12}	U_{13}	U_{23}
U1	0.0169(7)	0.0101(9)	0.0138(7)	0.0001(6)	0.0018(6)	–0.0012(6)
U2	0.0181(7)	0.0101(9)	0.0152(7)	0.0005(6)	0.0041(6)	0.0009(5)
U3	0.0227(8)	0.013(1)	0.0100(7)	0.0024(6)	0.0025(6)	0.0000(6)
U4	0.0230(8)	0.012(1)	0.0130(8)	–0.0017(6)	0.0070(6)	0.0005(6)
U5	0.0185(7)	0.0123(9)	0.0120(7)	–0.0005(6)	0.0044(5)	0.0025(6)
U6	0.0201(8)	0.0122(9)	0.0109(7)	0.0014(6)	0.0038(5)	–0.0002(6)
Pb1	0.0291(8)	0.0123(8)	0.0134(7)	0.0055(7)	0.0058(6)	0.0057(7)
Pb2	0.009(1)	0.047(2)	0.042(2)	0.019(2)	–0.0064(10)	–0.0018(12)
Pb3	0.015(2)	0.045(3)	0.036(2)	–0.002(2)	0.0088(14)	–0.007(2)
Pb4	0.027(2)	0.019(2)	0.034(2)	0.0048(14)	0.0156(14)	0.0056(14)
Pb5	0.019(4)	0.061(7)	0.045(5)	0.004(5)	0.016(4)	0.015(4)
Pb6	0.026(7)	0.083(14)	0.068(11)	–0.012(10)	0.023(7)	–0.029(8)

ianthinite and β-U_3O_8. The structural reason for the doubling of this parameter is the ordering of the Pb^{2+} cations in the interlayers (Fig. 5).

Miller et al. (1996) proposed a description of the anion topologies of layered uranyl oxide hydrates based on sequences of chains of polygons. Along this line, Burns (1999a) described the β-U_3O_8 anion topology as being composed of the chains **U**, **D**, and **R** with the repeat …**RUD**… (Fig. 4c). These chains are parallel to [021] in spriggite, and to [110] in ianthinite and β-U_3O_8.

TABLE 7. Selected bond lengths (Å) in the structure of spriggite

U1-O22	1.84(4)	Pb2-O22	2.67(4)
U1-O8	1.90(3)	Pb2-O6	2.73(3)
U1-O13	2.04(4)	Pb2-O22	2.76(3)
U1-O2	2.07(4)	Pb2-O5	2.80(3)
U1-O10	2.28(3)	Pb2-O3	2.83(3)
U1-O14	2.33(3)	Pb2-H_2O5	2.88(5)
<U1-O_{Ur}>	1.87	Pb2-O2	2.90(3)
<U1-O_{eq}>	2.18	Pb2-O6	2.95(3)
		<Pb2-φ>	2.82
U2-O19	1.73(3)		
U2-O9	1.90(3)	Pb3-O19	2.58(3)
U2-O12	2.07(3)	Pb3-O7	2.82(4)
U2-O1	2.09(3)	Pb3-O19	2.84(3)
U2-O15	2.28(3)	Pb3-O3	2.85(3)
U2-O18	2.40(3)	Pb3-H_2O2	2.87(1)
<U2-O_{Ur}>	1.82	Pb3-O15	2.95(3)
<U2-O_{eq}>	2.21	Pb3-O7	2.96(4)
		Pb3-O5	3.01(3)
U3-O7	1.76(3)	<Pb3-φ>	2.86
U3-O20	1.80(3)		
U3-O14	2.22(3)	Pb4-O20	2.74(3)
U3-O15	2.28(3)	Pb4-O20	2.76(3)
U3-O13	2.35(3)	Pb4-O21	2.79(3)
U3-O12	2.37(4)	Pb4-O21	2.82(3)
U3-OH16	2.39(3)	Pb4-O8	2.94(4)
<U3-O_{Ur}>	1.78	Pb4-O9	3.03(4)
<U3-φ_{eq}>	2.32	Pb4-O14	3.14(3)
		Pb4-H_2O4	3.19(12)
U4-O6	1.83(3)	Pb4-O12	3.23(3)
U4-O11	1.87(3)	<Pb4-φ>	2.96
U4-O10	2.20(3)		
U4-O18	2.24(3)	Pb5-O5	2.72(3)
U4-OH16	2.32(3)	Pb5-O19	2.75(4)
U4-O1	2.36(4)	Pb5-O3	2.75(3)
U4-O2	2.41(3)	Pb5-O6	2.80(4)
<U4-O_{Ur}>	1.85	Pb5-O6	2.83(4)
<U4-φ_{eq}>	2.31	Pb5-H_2O2	2.83(1)
		Pb5-O18	2.94(3)
U5-O3	1.79(3)	Pb5-O19	3.00(4)
U5-O21	1.85(2)	<Pb5-φ>	2.83
U5-O18	2.16(3)		
U5-O14	2.27(3)	Pb6-O22	2.51(4)
U5-OH17	2.36(3)	Pb6-O7	2.57(4)
U5-O2	2.37(4)	Pb6-O3	2.59(4)
U5-O12	2.38(3)	Pb6-H_2O5	2.76(5)
<U5-O_{Ur}>	1.82	Pb6-O22	2.98(4)
<U5-φ_{eq}>	2.31	Pb6-O5	3.04(4)
		Pb6-O7	3.12(4)
U6-O5	1.79(3)	<Pb6-φ>	2.80
U6-O4	1.83(3)		
U6-O15	2.25(3)	Pb7-H_2O1	2.02(12)
U6-O10	2.34(3)	Pb7-O8	2.30(4)
U6-OH17	2.37(3)	Pb7-O9	2.39(4)
U6-O1	2.37(3)	Pb7-H_2O4	2.60(12)
U6-O13	2.41(4)	Pb7-O20	2.66(4)
<U6-O_{Ur}>	1.81	Pb7-O21	2.68(4)
<U6-φ_{eq}>	2.35	Pb7-O4	2.88(4)
		Pb7-O11	2.88(4)
Pb1-H_2O1	2.19(5)	<Pb7-φ>	2.55
Pb1-O9	2.43(3)		
Pb1-O8	2.49(4)		
Pb1-H_2O3	2.51(6)		
Pb1-H_2O4	2.58(12)		
Pb1-O11	2.67(3)		
Pb1-O21	2.84(3)		
Pb1-O4	2.85(3)		
Pb1-O20	2.88(3)		
Pb1-O13	3.36(3)		
<Pb1-φ>	2.68		

Note: φ = O, OH, H_2O.

Comparison with hydrated Pb uranyl oxyhydroxide minerals

Spriggite is the eighth hydrated Pb uranyl oxyhydroxide known as a mineral species. The seven others are curite, fourmarierite, sayrite, richetite, masuyite, vandenriesscheite, and

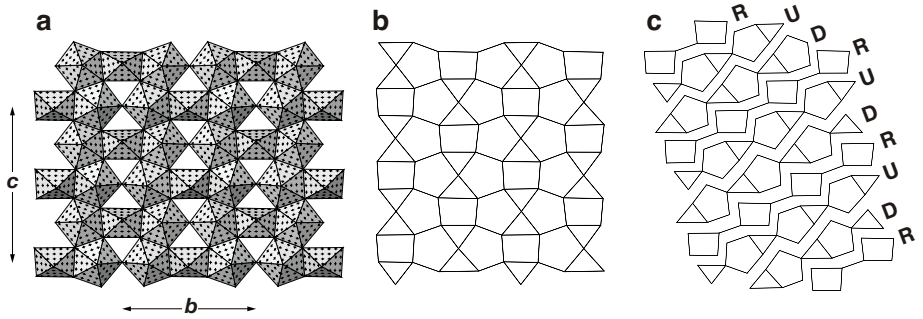

FIGURE 4. Projection of the sheet of uranyl polyhedra in the structure of spriggite along the *a* axis (**a**), its anion topology constructed according the method of Burns et al. (1996) (**b**), and construction of anion topology from the chains of polygons (**c**).

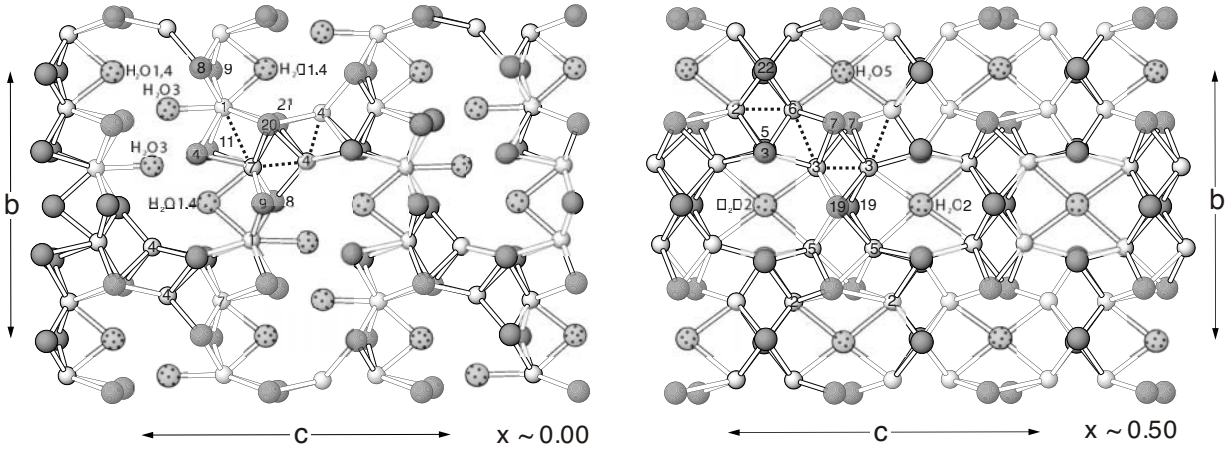

FIGURE 5. Structure of the interlayer in spriggite at the levels of $x \sim 0$ and $x \sim 1/2$.

wölsendorfite (Table 1). Finch and Ewing (1992) considered the sequence of hydrated Pb uranyl oxyhydroxides that form due to the alteration of uraninite under oxidizing conditions. According to Finch and Ewing (1992) and Finch and Murakami (1999), the reaction pathway for increasing alteration of hydrated Pb uranyl oxyhydroxides can be illustrated using the compositional diagram shown in Figure 6. The composition of a hydrated Pb uranyl oxyhydroxide is expressed as a sum xPbO + $y$$UO_3$ + $z$$H_2O$, where x, y, and z are molar proportions of PbO, UO_3, and H_2O, respectively ($x + y + z = 1$). The diagram in Figure 6 shows molar proportion of PbO (x) vs. molar proportion of H_2O (z). The arrow indicates increasing alteration of hydrated Pb uranyl oxyhydroxides according to Finch and Ewing (1992). It is interesting that, according to this diagram, spriggite is the most altered among known hydrated Pb uranyl oxyhydroxides. As it is clear from Table 1, it also has the highest Pb:U ratio. Burns (1997) described the sequence of crystal structures of hydrated Pb uranyl oxyhydroxides in terms of ratios Pb:U and U:(charge of sheet) (Table 1). In turn, the charge of the sheet is balanced through the $O^{2-} \rightarrow OH^-$ substitution (Burns 1997).

Table 1 also provides a $^{VI}U:^{VII}U$ ratio for the sheets of uranyl polyhedra in the structures of hydrated Pb uranyl oxyhydroxides. This ratio reflects the relative number of square and pentagonal uranyl bipyramids within the sheets. It is important to note that, with increasing Pb:U ratio (i.e., increasing Pb content), the $^{VI}U:^{VII}U$ ratio increases as well. This increase corresponds to the evolution of anion topologies of the uranyl polyhedra toward those with the higher number of squares. The anion topologies of vandenriesscheite, fourmarierite, masuyite, and richetite contain no squares ($^{VI}U:^{VII}U = 0$). The complex anion topology of the wölsendorfite sheet deciphered by Burns (1999b) contains squares. According to Burns (1999b), it consists of slabs of α- and β-U_3O_8 anion topologies ($^{VI}U:^{VII}U = 3:11$). The sayrite anion topology has $^{VI}U:^{VII}U = 1:4$, and can also be described as based on slabs of the α- and β-U_3O_8 anion topologies. The spriggite sheet is solely based upon the β-U_3O_8 anion topology. The curite anion topology ($^{VI}U:^{VII}U = 1:3$) is topologically different from those of wölsendorfite, sayrite, and spriggite. In particular, its construction requires another chain of polygons, $\mathbf{U^m}$, described by Burns (1999a).

As shown above, the anion topology of the sheets in hydrated Pb uranyl oxyhydroxides is related to the Pb content of the interlayer. The higher the Pb content, the higher the $^{VI}U:^{VII}U$ ratio. To explain this phenomenon, we suggest two possible mechanisms.

(1) The charge of the sheet is balanced by the $O^{2-} \rightarrow OH^-$ substitution (Li and Burns 2000b). The replacement of

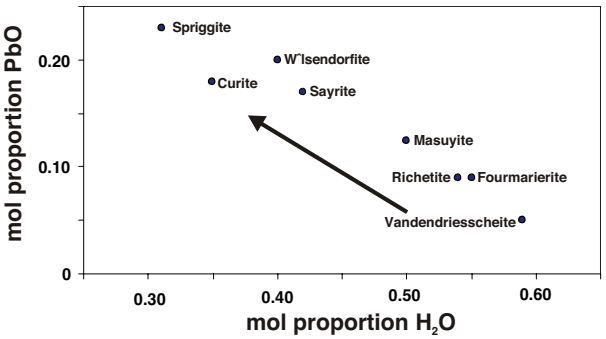

FIGURE 6. Compositional diagram illustrating the chemical evolution of hydrated Pb uranyl oxyhydroxides [modified from Finch and Murakami (1999)]. The arrow indicates increasing alteration of hydrated Pb uranyl oxyhydroxides.

OH^- by O^{2-} requires more bonding strength accumulated at the anion site to satisfy bond-valence requirements of the O^{2-} anion. The equatorial U^{6+}-O bonds in the UrO_4 square bipyramids are considerably shorter and of higher bond valence than the U^{6+}-O bonds in the UrO_5 pentagonal bipyramids. The change of the uranyl ion coordination from square to pentagonal helps to satisfy bond-valence requirements of O^{2-} in the anion site.

(2) The Pb atoms in the interlayer are coordinated mostly by the O atoms of uranyl ions and H_2O groups. Increasing the Pb content results in the formation of stronger Pb-O bonds, to satisfy the bond-valence requirements of Pb atoms. The latter favors elongation of U^{6+}-O_{Ur} bonds in uranyl ions, which decreases the bond valence to the O_{Ur} atoms from U. Burns et al. (1997a) demonstrated that the UrO_4 square bipyramids are more flexible than other U^{6+} coordinations and in some cases almost regular $U^{6+}O_6$ coordination may be achieved (cf., Li et al. 2001). Thus, the increase in the ^{VI}U:^{VII}U ratio helps to satisfy bond-valence requirements of the Pb atoms in the interlayer.

It is likely that aforementioned mechanisms (1) and (2) are equally important in determining evolution of anion topologies with the increase in the Pb content in hydrated Pb uranyl oxyhydroxides.

Relationship between spriggite and other uranium alteration minerals

The chemical and structural characterization of spriggite shows its unique position among the known hydrated Pb uranyl oxyhydroxides as the mineral with the highest Pb:U and ^{VI}U:^{VII}U ratios. Spriggite is another example of the ability of the β-U_3O_8 type sheet to host U atoms with a variety of oxidation states (U^{4+}/U^{6+} in ianthinite; U^{5+}/U^{6+} in β-U_3O_8; U^{6+} only in billietite and spriggite). The composition and configuration of the interlayer seems to be the main factor stabilizing a particular oxidation state for U in the sheet. This aspect must be taken into account when considering phases such as ianthinite as possible hosts for Pu during the alteration of Pu-bearing waste (Burns et al. 1997b). The high Pb:U and ^{VI}U:^{VII}U ratios in spriggite can be related to the geology of the occurrence: deep weathering favored full oxidation of U, and the alteration of an unidentified U- and Pb-rich primary phase provided the high Pb concentrations that are probably required to stabilize spriggite in the weathering environment.

ACKNOWLEDGMENTS

The partial financial support for S.V.K. was provided by the INTAS postdoctoral fellowship and the fellowship from the Alexander von Humboldt foundation (project "Crystal Chemistry of Minerals and Inorganic Compounds with Lone Electron Pair cations"). J.B. acknowledges an Australian Research Council Queen Elizabeth II fellowship. We thank the Sprigg family for welcoming us onto their property, and I. Plimer for introducing us to the secrets of Flinders Ranges. We thank Philippe Thélin and P.O. Baumgartner, Unversity of Lausanne, for powder XRD, FT-IR, and SEM imaging facilities. The paper benefited from insightful reviews by R. Finch, Y. Li, and P. Burns.

REFERENCES CITED

Burns, P.C. (1997) A new uranyl oxide hydrate sheet in vandendriesscheite—Implications for mineral paragenesis and the corrosion of spent nuclear fuel. American Mineralogist, 82, 1176–1186.

——— (1998) The structure of richetite, a rare lead uranyl oxide hydrate. Canadian Mineralogist, 36, 187–199.

——— (1999a) The crystal chemistry of uranium. In P.C. Burns and R. Finch, Eds., Uranium: Mineralogy, geochemistry and the environment, 38, p. 23–90. Mineralogical Society of America, Blacksburg, Victoria.

——— (1999b) A new complex sheet of uranyl polyhedra in the structure of wölsendorfite. American Mineralogist, 84, 1661–1673.

Burns, P.C. and Finch, R.J. (1999) Wyartite: Crystallographic evidence for the first pentavalent-uranium mineral. American Mineralogist, 84, 1456–1460.

Burns, P.C. and Hanchar, J.M. (1999) The structure of masuyite, $Pb[(UO_2)_3O_3(OH)_2](H_2O)_3$, and its relationship to protasite. Canadian Mineralogist, 37, 1483–1491.

Burns, P.C., Miller, M.L., and Ewing, R.C. (1996) U^{6+} minerals and inorganic phases; a comparison and hierarchy of crystal structures. The Canadian Mineralogist, 34, 845–880.

Burns, P.C., Ewing, R.C., and Hawthorne, F.C. (1997a) The crystal chemistry of hexavalent uranium: polyhedron geometries, bond-valence parameters, and polymerization of polyhedra. Canadian Mineralogist, 35, 1551–1570.

Burns, P.C., Finch, R.J., Hawthorne, F.C., Miller, M.L., and Ewing, R.C. (1997b) The crystal structure of ianthinite, $[U_2^{4+}(UO_2)_4O_6(OH)_4(H_2O)_4](H_2O)_5$—a possible phase for Pu^{4+} incorporation during the oxidation of spent nuclear fuel. Journal of Nuclear Materials, 249, 199–206.

Cejka, J. (1999) Infrared spectroscopy and thermal analysis of uranyl minerals. In P.C. Burns and R. Finch, Eds., Uranium: Mineralogy, geochemistry and the environment, 38, 521–622. Mineralogical Society of America, Blacksburg, Victoria.

Coats, R.P. and Blissett, A.H. (1971) Regional and economic geology of the Mount Painter province. Department of Mines, Geological Survey of South Australia, Bulletin 43, 426 pp.

Colon, C.F.J., Brady, P.V., Siegel, M.D., and Lindgren, E.R. (2001) Historical case analysis of uranium plume attenuation. Soil & Sediment Contamination, 10, 71–115.

Elburg, M., Bons, P., Foden, J., and Brugger, J. (2003) A newly defined Late Ordovician magmatic-thermal event in the Nt Painter Province, nothern Flinders Ranges, South Australia. Australian Journal of Earth Sciences, 50, 611–631.

Ewing, R.C. (1993) The long-term performance of nuclear waste forms: natural materials—three case studies. Materials Research Society Symposium Proceedings, 294, 559–568.

Finch, R. and Murakami, T. (1999) Systematics and paragenesis of uranium minerals. In P.C. Burns, and R. Finch, Eds., Uranium: Mineralogy, geochemistry and the environment, 38, p. 91–179. Mineralogical Society of America, Blacksburg, Victoria.

Finch, R.J. and Ewing, R.C. (1992) The corrosion of uraninite under oxidizing conditions. Journal of Nuclear Materials, 190, 133–156.

———(1994) Formation, oxidation and alteration of ianthinite. In A. Barkatt, and R.A. Van Konynenburg, Eds., Scientific basis for nuclear waste management XVII., 333, p. 625–630. North-Holland, New York-Amsterdam-Oxford, United States of America.

Foster, D.A., Murphy, J.M., and Gleadow, A.J.W. (1994) Middle Tertiary hydrothermal activity and uplift of the Northern Flinders Ranges, South Australia—Insights from apatite fission-track thermochronology. Australian Journal of Earth Sciences, 41, 11–17.

Ibers, J.A. and Hamilton, W.C. (1974) International Tables for X-ray crystallography, vol. IV. The Kynoch Press, Birmingham, U.K.

Idnurm, M. and Heinrich, C.A. (1993) A palaeomagnetic study of hydrothermal activity and uranium mineralisation at Mt Painter, South Australia. Australian Journal of Earth Sciences, 40, 87–101.

Krivovichev, S.V. and Brown, I.D. (2001) Are the compressive effects of encapsulation an artifact of the bond valence parameters? Zeitschrift für Kristallographie, 216, 245–247.

Li, Y. and Burns, P.C. (2000a) Investigations of crystal-chemical variation in lead uranyl oxide hydrates. I. Curite. Canadian Mineralogist, 38, 727–735.

——— (2000b) Investigations of crystal-chemical variation in lead uranyl oxide

hydrates. II. Fourmarierite. Canadian Mineralogist, 38, 737–749.
Li, Y., Cahill, C.L., and Burns, P.C. (2001) Synthesis, structural characterization, and topological rearrangement of a novel open framework U-O material: $(NH_4)_3(H_2O)_2\{[(UO_2)_{10}O_{10}(OH)][(UO_4)(H_2O)_2]\}$. Chemistry of Materials, 13, 4026–4031.
Loopstra, B.O. (1970) The structure of β-U_3O_8. Acta Crystallographica, B26, 656–657.
Mereiter, K. (1979) The crystal structure of curite, $[Pb_{6.56}(H_2O,OH)_4][(UO_2)_8O_8(OH)_6]_2$. Tschermaks Mineralogische und Petrographische Mitteilungen, 26, 279–292.
Miller, W., Alexander, R., Chapman, N., McKinley, I., and Smellie, J. (2000) Geological disposal of radioactive wastes and natural analogue. Pergamon Press, Oxford, 320 p.
Miller, W., Finch, R.J., Burns, P.C., and Ewing, R.C. (1996) Description and classification of uranium oxide hydrate sheet anion topology. Journal of Materials Research, 11, 3048–3056.
Pagoaga, M.K., Appleman, D.E., and Stewart, J.M. (1987) Crystal structures and crystal chemistry of the uranyl oxide hydrates becquerelite, billietite, and protasite. American Mineralogist, 72, 1230–1238.
Pearcy, E.C., Prikryl, J.D., Murphy, W.M., and Leslie, B.W. (1994) Alteration of uraninite from Nopal I Deposit, Pena Blanca District, Chihuahua, Mexico, compared to degradation of spent nuclear fuel in the proposed U.S. high-level nuclear waste repository at Yucca Mountain, Nevada. Applied Geochemistry, 9, 713–732.
Piret, P. (1984) Structure cristalline de la fourmariérite, $Pb(UO_2)_4O_3(OH)_4{\cdot}4H_2O$. Bulletin de la Société française de Minéralogie et Cristallographie, 108, 659–665.
Piret, P., Deliens, M., Piret-Meunier, J., and Germain, G. (1983) La sayrite, $Pb_2[(UO_2)_5O_6(OH)_2]{\cdot}4H_2O$, nouveau minéral; propriétés et structure cristalline. Bulletin de la Société française de Minéralogie et Cristallographie, 106, 299–304.
Sandiford, M., Hand, M., and McLaren, S. (1998) High Geothermal Gradient Metamorphism During Thermal Subsidence. Earth & Planetary Science Letters, 163, 149–165.
Smith, R.E. (1996) Regolith research in support of mineral exploration in Australia. Journal of Geochemical Exploration, 57, 159–173.
Walker, S. (1999) Beverley Uranium Project—in situ mining approved. MESA Journal, 13, 8–10.

MANUSCRIPT RECEIVED MARCH 20, 2003
MANUSCRIPT ACCEPTED OCTOBER 22, 2003
MANUSCRIPT HANDLED BY PETER BURNS